# CCAT-prime/FYST: A status report on the ultra-widefield submillimeter observatory on Cerro Chajnantor

G.J. Stacey<sup>1</sup>, Nicholas Battaglia<sup>1</sup>, Scott C. Chapman<sup>2</sup>, Steve K. Choi<sup>1</sup>, Laura M. Fissel<sup>3</sup>, Urs Graf<sup>4</sup> Terry Herter<sup>1</sup>, Douglas Johnstone, <sup>5,6</sup>, P. Daniel Meerburg<sup>6</sup>, Michael D. Niemack<sup>1</sup>, Thomas Nikola<sup>1</sup>, Stephen Parshley<sup>1</sup>, Dominik A. Riechers<sup>4</sup>, Robert Simon<sup>4</sup>, Eve M. Vavagiakis<sup>1</sup> and the CCAT-prime Collaboration.

<sup>1</sup>Cornell University, Ithaca, NY 14805, US, <sup>2</sup>Dalhousie University, Halifax, NS B3H4R2, Canada,
<sup>3</sup>Queen's University, Kingston, ON K7L 3N6, Canada, <sup>4</sup>Universität zu Köln, Zülpicher Str. 77, D-50937 Köln, Germany, <sup>5</sup>National Research Council Canada, 5071 West Saanich Road, Victoria, BC,V9E 2E7, Canada, <sup>6</sup>University of British Columbia, Vancouver, BC V6T1Z1, Canada
<sup>7</sup>University of Groningen, Nijenborgh 4, 9747 AG Groningen, The Netherlands

#### Abstract

We report on the CCAT-prime Project, including the science program, the Fred Young Submillimeter Telescope (FYST), its instrumentation, and the schedule. FYST is a 6-m telescope sited at 5600 m elevation near the summit of Cerro Chajnantor in northern Chile. The site, together with its very large field-of-view optics, and high surface accuracy, low-emissivity surface enables pursuit of low surface brightness science over large fields. Our science goals include: tracing the formation and evolution of star forming galaxies from the epoch of reionization to the cosmic peak of star formation activity through wide-field, broad-band [CII] line imaging and dust continuum surveys; constraining thermodynamics and feedback in galaxy clusters through the Sunyaev-Zel'dovich effects on the CMB; improving constraints on primordial gravitational waves through precision removal of polarization foregrounds; and tracing local star formation processes through velocity-resolved spectroscopy at 15" spatial resolution over 110° scales in the Galaxy. These goals are realized through sensitive wide-field surveys. Our main instruments are Prime-Cam, a large FoV direct detection imager and CHAI, a multi-beam submillimeter heterodyne spectrometer. We have also built Mod-Cam which serves as a Prime-Cam test facility and/or first light camera. Prime-Cam has seven instrument modules, four now under construction: three polarimetric cameras (at 280, 350, and 850 GHz) and a 210-420 GHz Fabry-Perot imaging spectrometer, EoR-Spec. CHAI will have 128 pixels covering important lines in the short submillimeter windows.

The CCAT-prime team is an international group of universities, led by Cornell University. FYST is being designed and built by CPI Vertex Antennentechnik, GmbH, Germany with first light expected in 2024.

**Keywords:** Submillimeter telescope, CCAT-prime, Prime-Cam, Mod-Cam, CHAI, Epoch of Reionization, Sunyaev-Zel'dovich effect, high redshift galaxies, star formation, dusty star forming galaxies

# 1. INTRODUCTION

The CCAT-prime collaboration is an international group of educational institutions and research institutes brought together by the desire to pursue high surface brightness sensitivity science in the submillimeter to millimeter wave bands. The collaboration is led by Cornell University and consists of Cornell University, a German consortium consisting of the University of Cologne, the University of Bonn, and the Max Planck Inst. for Astrophysics which is led by the University of Cologne, and the Canadian Atacama Telescope Corp (CATC) consisting of the Universities of Waterloo, Toronto, British Columbia, Calgary, Dalhousie, McGill, McMaster, and Western Ontario that is led by the University of Waterloo. Cornell and the German Consortium together form CCAT Corporation, and CCAT is a Joint Venture between CCAT Corporation & CATC. Science topics run from efforts to understand fundamental physics through detailed polarimetric imaging of the Cosmic Microwave Background (CMB) through studies of star formation in the Milky Way galaxy. These topics are best pursued with a very wide field-of-view (FoV), low-emissivity telescope placed at a suberb site, and equipped with a suite of state-of-the-art widefield instrumentation.

We list the eight primary science themes that are uniquely addressed through instrumentation available on the FYST telescope below, together with brief summaries of the expected science yield for each one. Our science themes are:

- 1. Line Intensity Mapping: Trace the reionization of the Universe and galaxy evolution through line intensity mapping.
- Galaxy Evolution: Explore the evolution of dusty star forming galaxies across cosmic time through submillimeter continuum surveys.
- 3. **Cluster Evolution:** Trace the growth of large-scale structures, reveal fundamental physics, and constrain the intracluster gas thermodynamics and feedback in galaxy clusters through Sunyaev-Zel'dovich effect distortions of the CMB.
- 4. **Cosmological Foregrounds**: Improve searches for primordial gravity waves through deep submillimeter polarization measurements of the cosmic microwave background (CMB) and using multi-band high frequency polarimetry to correct for polarized emission from foreground Galactic dust.
- 5. Rayleigh Scattering: Measure structure evolution throughout the recombination epoch through Rayleigh Scattering.
- 6. **Galactic Polarization:** Trace the influence of magnetic fields on star formation processes in the Milky Way and local galaxies through submillimeter polarimetry
- 7. Galactic Ecology: Trace the physical properties and velocity fields of neutral gas associated with star formation processes in the Milky Way and local galaxies through velocity-resolved spectroscopy of submillimeter molecular and fine-structure lines.
- 8. **Time Domain Astrophysics:** Monitor astrophysical sources in the time-domain tracing for example the time evolution of supernovae, gamma-ray bursts, tidal disruption events, and accretion luminosity of protostars.

We discuss several of these goals in greater detail in Section 5 below. For further information on each of these science cases, we refer the reader reference [1].

# 2. THE FRED YOUNG SUBMILLIMETER TELESCOPE [2],[3]

The Fred Young Submillimeter Telescope (FYST) is a 6 m aperture unobscured telescope in a crossed Dragone configuration ([4], [5], Figure 1) held within an altitude-azimuth fork mount (Figure 2, left). The primary mirror is tipped with respect to its principal ray such that it sends the rays from sources on the sky to a large secondary mirror on the elevation axis. From here, the secondary sends the beam back across the primary to form an image plane at the elevation bearing in the opposite fork. The field produced by this optical configuration is flat and has an exceptionally large diffraction-limited elliptically shaped field of view that is up to an  $8.0^{\circ} \times 6.4^{\circ}$ ,  $5.1^{\circ} \times 4.1^{\circ}$ , and  $2.1^{\circ} \times 2.6^{\circ}$  in size at 3.0, 1.3, and 0.35-mm wavelengths respectively. FYST was designed by, and being built by CPI Vertex Antennentechnik, GmbH, Germany.

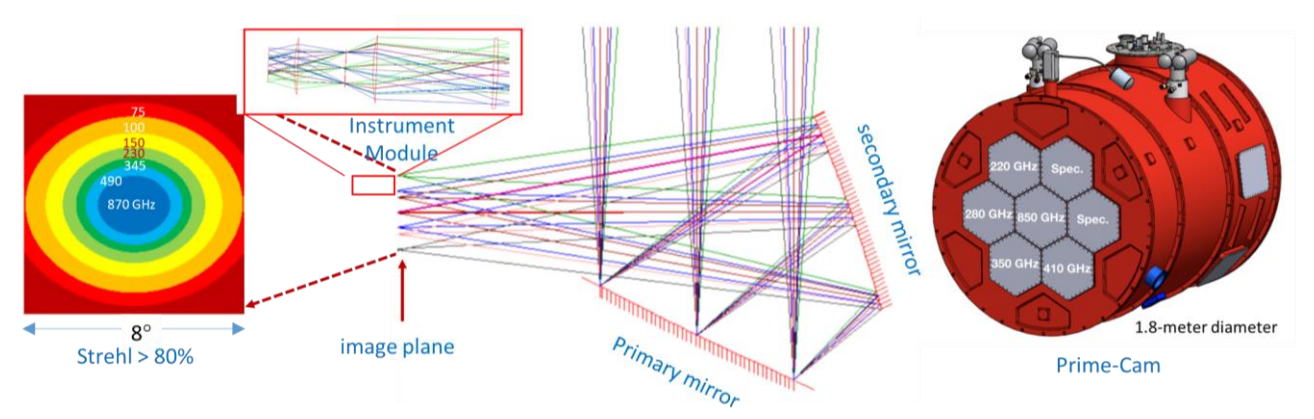


**Figure 1.** (center) Optical diagram for the FYST telescope illustrated with point sources at 7 positions in an 8° field of view. Up to 7 instrument modules (small red rectangle to the left of the image plane) can be held in our direct detection focal plane instrument, Prime-Cam (right, Section 3.1). Notional positions of the planned 7 modules are indicated on its entrance windows. The enlarged version of an instrument module (insert above the red rectangle) shows a typical instrument module optical system that is based on 3 lenses and a pupil for stray light control. (left) The FYST Strehl ratio in the image plane is better than 80% for a field size of 2.6° and 8° at 850 and 100 GHz (or 0.35 mm and 2 mm wavelength) respectively.

The FYST telescope is designed to achieve a very small wavefront front error (<10.7  $\mu m$  rms) so as to achieve high aperture efficiencies deep into the short submillimeter bands ( $\lambda < 350~\mu m$ ; v > 850~GHz). The high accuracy requires the use of Invar in the truss structure of the elevation housing and a carbon-fiber based backing structure for both the primary and secondary mirrors. The mirrors themselves are light weighted aluminum panels diamond machined to better than 3.5  $\mu m$  rms surface accuracy. There are 77 mirror segments in the primary, and 69 in the secondary. The panels are set to have very small gaps (requirement < 2 mm) such that the overall emissivity requirement for the telescope of < 2.8% can be attained. The telescope can scan at up to 3°/sec in azimuth and 1.5°/sec in elevation on track and achieve 1/10 beam pointing knowledge during scans at even our shortest nominal wavelength, 350  $\mu m$  where the beam size is 15" (FWHM). The telescope can also observe in the elevation rage from 0 to 170° so that, for example, polarization systematics can be minimized by observing sources with the system optics rotated on the sky.

Since FYST is designed to operate in the 350  $\mu$ m to 3 mm telluric windows, the choice of site is paramount. FYST will be sited at 5600 m elevation near the summit of Cerro Chajnantor in northern Chile – 600 meters above ALMA, which is on the superb Chajnantor plateau site. The additional 600 meters in elevation gains quite significantly in sensitivity due to significantly improved median water vapor burden. The burden drops from 1.0 mm on the plateau to 0.6 mm at the 5600 m elevation FYST site which greatly (factor of 4) improves mapping speed at high frequencies (850 GHz  $\Leftrightarrow$  350  $\mu$ m) and still significantly (factor of 1.4) improves mapping speeds at 220 GHz, our lowest planned frequency for Prime-Cam (Figure 2, right). Our science program is enabled by the low water vapor burden of the site, the large field of view of the FYST crossed-Dragone optical design, its high surface accuracy, and the low emissivity of the FYST telescope that combine to yield exceptionally large mapping speeds.

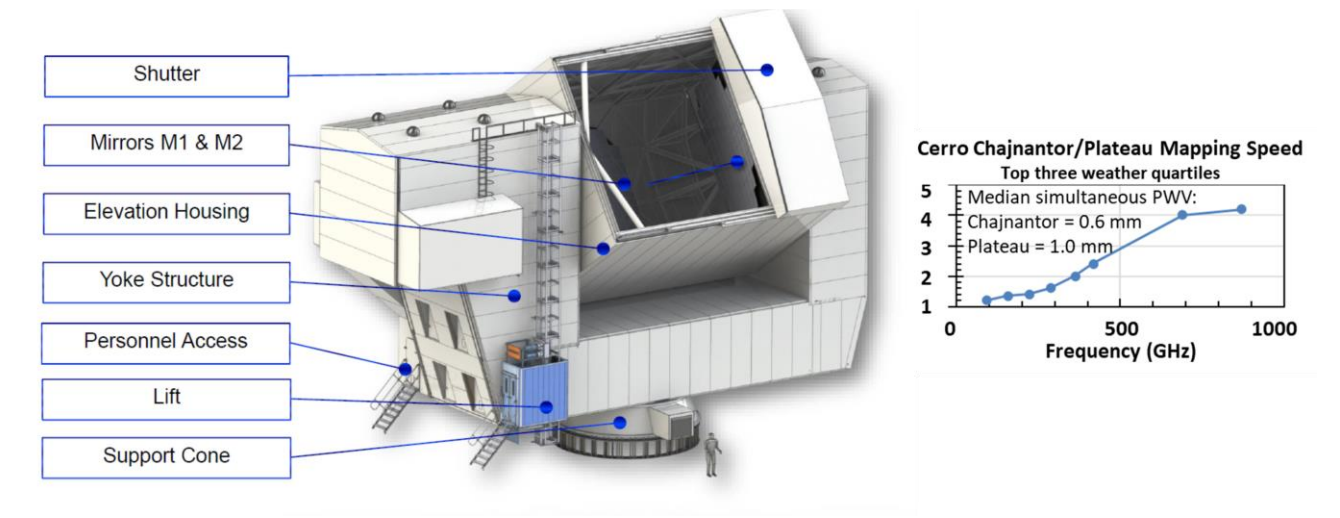


**Figure 2.** (left) The FYST altitude-azimuth fork mount design. The design features a retractable shutter, 170° range in elevation and two instrument spaces within the left (in this view) yoke arm. Instrument Space 1 (IS1) is on the Naysmuth optical axis and directly feeds Prime-Cam. Instrument Space 2 (IS2) is one level below IS1 and houses CHAI. CHAI is serviced by a pick-off mirror and optical system (Section 3.4) that can be remotely installed in front of Prime-Cam. (right) The relative mapping speed as a function of observing frequency for identical instruments on FYST if the system were at the FYST site on Cerro Chajnantor compared to placement at the ALMA plateau site. The FYST site at 5600 m elevation provides up to a factor of four mapping speed advantage.

# 3. INSTRUMENTATION

The CCAT-prime science program is delivered by two distinct instruments: Prime-Cam, which is a wide-field of view direct detection imaging system based on arrays of Kinetic Inductance Detectors (KIDS) and the CCAT Heterodyne Array Instrument (CHAI), which is a multi-beam, two band submillimeter heterodyne receiver.

# 3.1 Prime-Cam [6], [7]

The FYST field of view needs to be split into smaller sections so that the entrance windows to the instruments (each made of UHMWPE) are small enough to bear atmospheric pressure. We split the focal plane into 7 independent instrument modules with 40 cm diameter entrance windows, each accepting a 1.3° field of view (Figure 1). The overall

field of view intercepted by Prime-Cam is 4.9°. Each instrument module is 42.3 cm in diameter and 120.8 cm long. The modules contain the requisite silicon lenses – which have been anti-reflection coated with a metamaterial layer, baffles, Lyot stop, and optical filtration (see Figure 1) to deliver the required science frequencies and spectral purity onto a diffraction limited image plane. The instrument focal plane is cooled to < 100 mK with a Bluefors model DL400 dilution refrigerator, and a series of pulse tube coolers from Cryomech cool the instrument modules and several radiation shields.

# 3.2 Focal planes [8], [9], [10], [11], [12], [13].

The focal planes within each instrument module are large format Microwave Kinetic Inductance arrays from NIST. Arrays based on this technology have been tested in the lab and used on the sky, where they demonstrated sensitivities that indicate our camera and spectrometer arrays in Prime-Cam will be background limited. [14], [15]. Focal planes within each tube consist of three closely abutted arrays each of which is made on 6-inch silicon wafers (Figure 3). Each of these wafers has > 1000 (depending on frequency) diffraction-limited beams. Each spatial pixel will be feedhorn-fed and coupled to a waveguide that sends the EM wave to an inductor that absorbs the wave energy. For the polarimetric cameras, each polarization is detected by an independent KID, while for EoR-Spec both polarizations are tied together so that only one KID is required for each spatial position on the sky.

At present, four instrument modules are fully funded and under construction: the 850 GHz, 350 GHz, and 280 GHz polarimetric camera modules, and one of the two planned EoR-Spec modules. The 850 GHz polarimetric camera module is under development within CATC at the University of British Columbia [16], [17]. It occupies the central position of Prime-Cam where the focal plane image quality is sufficient to ensure diffraction limited operation at this high frequency. This module contains 41,400 KID detectors, one at each polarization at 20,700 spatial positions on the sky. The detectors are fed by three silicon feedhorn arrays. The 280 and 350 GHz polarimetric camera modules are being developed at Cornell University and contain 10,350 KID detectors, one at each polarization at 5,175 spatial positions on the sky [1]. The 280 GHz module will have one metal and two silicon feedhorn arrays, while the 350 GHz module will be serviced by 3 silicon feedhorn arrays. EoR-Spec is being developed at Cornell University. Each module will have 6528 dual polarization KIDs. The focal plane is two color. Two of the three focal plane arrays center at 260 GHz, and combine to 3456 spatial positions on the sky, and the other array is centered at 370 GHz and will have 3072 spatial positions on the sky (see Figure 4 (right)). The EoR-Spec arrays will be fed by metal feedhorn arrays [10].

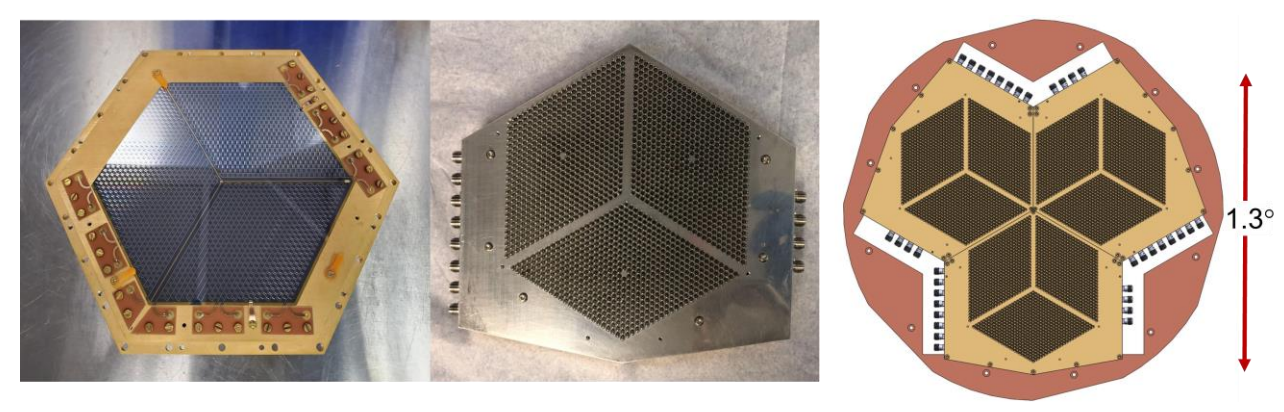


**Figure 3.** (left) Our first 280 GHz MKID array from NIST. Each array is formed on a 6" silicon wafer and spit into three parts to enable readout traces. (center) Array assembled for mechanical testing. (right) Each focal plane is constructed by closely abutting 3 arrays to fill out the 1.3° FoV [9].

# 3.3 EoR-Spec [18]

EoR-Spec is optimized for line intensity mapping (LIM) of the faint [CII] fine-structure line emission from galaxies at redshifts between 8 and 3.5 (Section 5.2). This is a very challenging program requiring broad-band (210 to 420 GHz) moderate resolving power ( $R = \lambda/\Delta\lambda > 100$ ) spectroscopy over degree-scale fields at the very high surface brightness sensitivity. The faintness of the expected signals necessitates that minimization of system systematics will also be very important. This instrumental challenge condenses down to maximizing pixel counts (spatial plus spectral) on the sky withing a high throughput, background limited system. Theoretical models of line emission in the early Universe suggest that to have high probability of success in the observations requires minimum pixel counts of order 5000 to 10,000. The large pixel counts can be obtained with a variety of technologies including Rowland-style grating

spectrometers [19], Fourier Transform spectrometers (FTS, [20]) and "spectrometer on chip" based technologies [21] [22]. The Rowland-style gratings and FTS-based systems are mature technologies, but the former suffers from challenges scaling up to the requisite numbers of beams on the sky, and the later can suffer from sky noise. The spectrometer on a chip technology can easily provide the beam-count but these systems are at present still an emerging technology. We chose a Fabry-Perot based spectrometer for EoR-Spec since it promises cross-linked spectral and spatial multiplexing, has inherently large throughput and both the FPI and the focal planes required are mature technologies.

Our EoR-Spec FPI is based on a flex-vane parallel translation stage used in previous generations of FPI-based instruments members of our team have created ([23], [24], [25], [26]). A significant improvement to these designs is that we plan to use silicon-substrate based mirrors in the etalon which should significantly improve performance over the broad bandwidth we require [27], [18], [28]. The translation stage is driven by a cryogenic stepper motor, and mirror spacing in the cavity is monitored through commercially available capacitive sensors. The 14 cm aperture FPI is placed in a 13 cm diameter pupil of the system in order to achieve the requisite resolving power of 100 over the entire 1.3° FoV.

Details of the FPI operation are shown in Figure 4. Off-axis rays going through a FPI see a different resonant wavelength (to the blue) than the on-axis rays. This means that at any given etalon gap, there will be a radially symmetric shift of imaged frequencies across the image plane. This is an advantage to the system: there is both spatial and spectral multiplexing at each setting of the FPI etalon. To create a uniform spectral scan, we set our Fabry Perot in 2<sup>nd</sup> order at 210 GHz, so the 3<sup>rd</sup> order fringe is at 315 GHz. We then scan spatially over the sky to ensure good sky coverage for the LIM fields, which are approximately 4 square degrees each in size. This will produce a data cube with a full sampling in the spatial dimension, and sampling in the spectral dimension extending over about 24 GHz, or about 11 spectral resolution elements at 210 GHz. We then move the FPI to higher frequencies by about 7 GHz and repeat the sky scanning. About 14 such steps in frequency ensure full spectral coverage in each 105 GHz wide bands. For more details on EoR-Spec, its overall design, optical design, array design and mirror technologies see [18], [27], [29], [10], [12], [28].

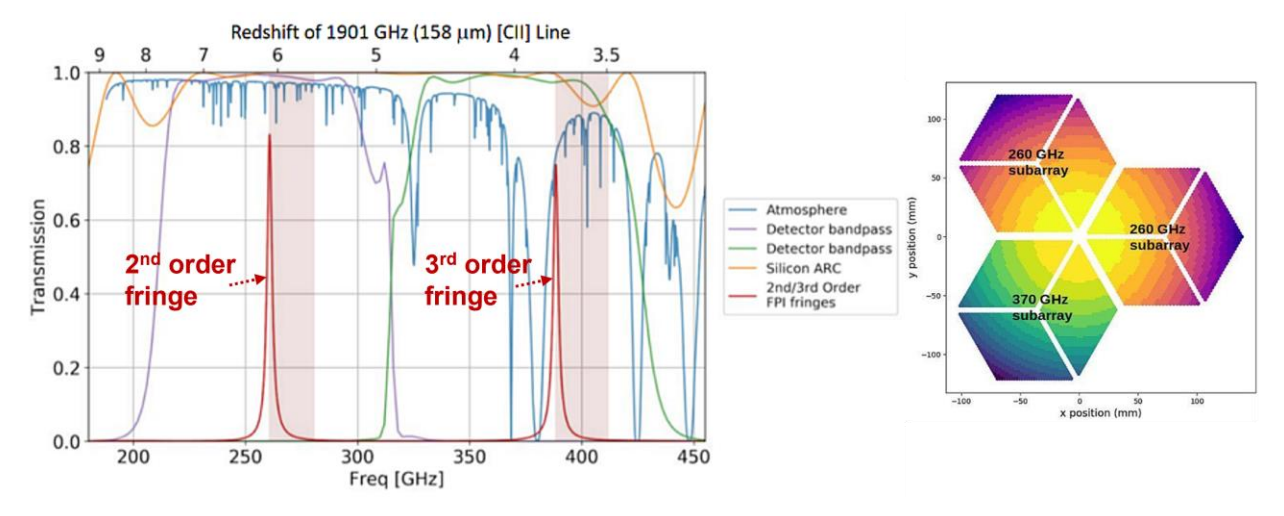


**Figure 4.** (left) Obtaining the spectrum over wide fields with EoR-Spec. Scanning is described in the text. Here we illustrate the case where the FPI is set at 260 GHz in 2<sup>nd</sup> order for the on-axis beams, so it also resonates at 390 GHz in third order (red Lorentzian profiles). The pink shaded regions illustrate the spectral extent covered at this setting by other, more off-axis beams in the focal plane array. The two fringes are resolved from one another by detector bandpasses (purple and green near- rectangular traces) set by a low frequency pass filter in front of the arrays, and the high frequency pass filtering capabilities of the condensing cones. The blue trace in the background is the telluric transmission at 45° elevation at the FYST site. The axis label at the top shows the redshift for [CII] line emission that corresponds to the frequency scanned as marked on the lower-level x-axis label. (right) The EoR-Spec focal plane. Two arrays are populated with detectors with bandpasses centered at 260 GHz, and the third is populated with detectors with bandpasses centered at 370 GHz. The higher areal coverage at 260 GHz is required by more challenging science demands of higher redshift line emission [18].

Table 1: Expected Sensitivities for Prime-Cam polarimetric cameras on FYST											
Instrument Module	v (GHz)	Δν (GHz)	Beam [arcsec]	N <sub>det</sub> (2 per beam, 1 per polarization)	NEI [Jy sr-¹√s]	NEFD/beam [mJy√s/beam]	NET [uK√s]				
220 GHz	220	56	59	7,938	3300	14/17/23	6.8				
280 GHz	280	60	47	10,350	5500	16/21/30	13				
350 GHz	350	35	37	10,350	14600	37/52/94	48				
410 GHz	410	30	32	20,808	37300	66/120/230	182				
850 GHz	850	97	15	41,400	479000	170/400/1700	310000				

# **Expected Sensitivities for EoR-Spec**

EoR Spec (2 modules)	v (GHz)	Δν (GHz)	Beam [arcsec]	N <sub>det</sub> (1 per beam, dual polarization)	NEI [Jy sr¹√s]	NEFD/beam [mJy√s/beam]	
210 to 315 GHz band	220	2.2	58	6912 spatial positions in the 210–315 GHz band	13,000	68/81/110	
	280	2.8	48		18,000	64/81/120	
315 to 420 GHz band	350	3.5	37	6144 spatial positions in the 315–420 GHz band	53,000	100/140/260	
	410	4.1	33		98,000	140/230/470	

Notes: NET temperatures are given in CMB units. Calculations assume a conservative 80% yield for the detectors. NEI and NET sensitivities are weighted averages of the top three weather quartiles. NEFDs is quoted for Q1/Q2/Q3. The values are 0.36, 0.67 and 1.28 mm zenith participable water vapor in Q1, Q2, and Q3 respectively. More details are in [1].

# 3.3.1 Performance

Noise models are based on the photon noise formulism in [31] degraded by the expected detector noise in quadrature, then further degraded by the noise angular power spectrum in the atmosphere (aka sky noise). The expected sensitivities are presented in [7], updated in [1] and summarized in Table 1 above.

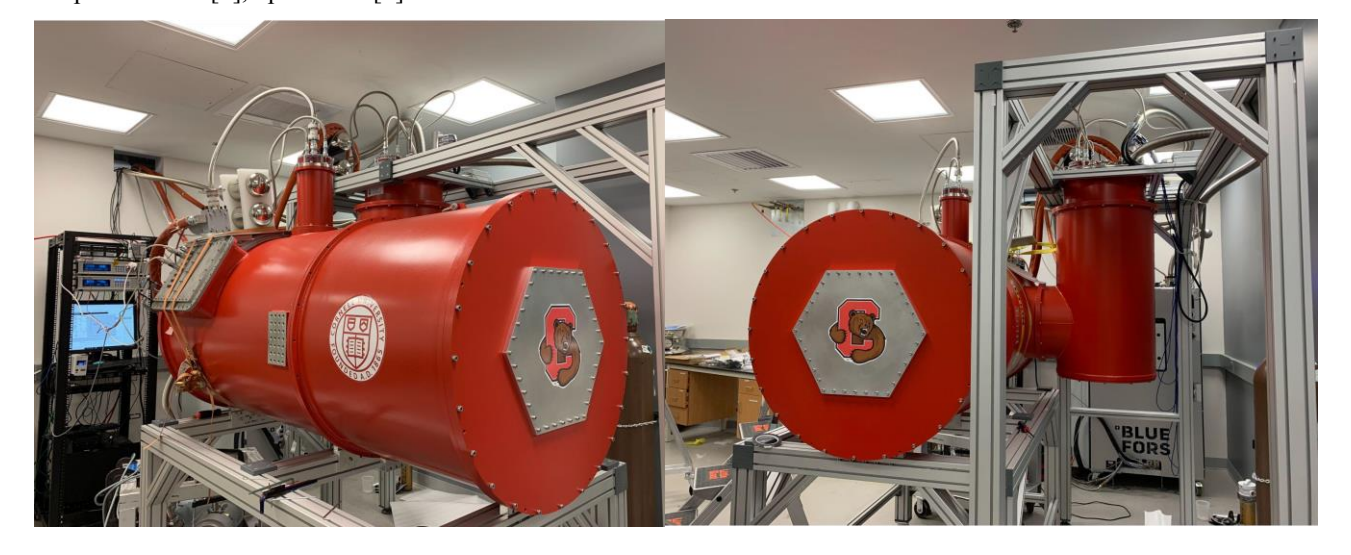


**Figure 5.** Two views of Mod-Cam. The left view illustrates the science instrument readout and pulse tube ports, and the right view highlights the (large vertical cylinder) Bluefors dilution refrigerator. The hexagonal port on the front of the main cryostat (horizonal) cylinder is the entrance window (in operation made of UHMWPE) but closed in these photographs for cryogenic tests. [30].

# 3.3.2 Mod-Cam: testing and possible first light instrument [30]

Prime-Cam is a complex, large format instrument. The cryostat itself is in manufacture by Redline Chamber and set to be delivered in the early fall of 2022, only about 15 months before the expected first light on FYST at its Cerro Chajnantor site. In addition, while it is clear that the 280 GHz module will be ready for first light, it is not clear how many if any other instrument modules will also be ready for first light. We have therefore developed an additional, smaller cryostat, called Mod-Cam (Figure 5). Mod-Cam is built, in the lab, and has undergone extensive cryogenic testing and now is ready for instrument module level tests [30]. If only the 280 GHz instrument module is ready for first light, it will be installed in Mod-Cam and sent to the telescope. If Prime-Cam is ready, and more than one instrument module is ready at first light, we will likely send the more capable Prime-Cam system down to the site for first light and hold Mod-Cam back to assist in the development and test of further instrument modules. At any rate, we expect Mod-Cam will serve as the long-term test cryostat to ready instrument modules for insertion into Prime-Cam at the site, and on the telescope.

# 3.4 CHAI [32]

CHAI (Figure 6) is a dual band heterodyne array spectrometer under construction at the University of Cologne [32] The low frequency band (LFB) covers 455 to 495 GHz so that the [CI]  ${}^{3}P_{1} \rightarrow {}^{3}P_{0}$  (492 GHz) fine-structure transition and  ${}^{12}CO(4\rightarrow 3)$  (460 GH) lines are available for observations in the Milky Way galaxy and local galaxes, and the high frequency band (HFB) covers 800 to 820 GHz so that the [CI]  ${}^{3}P_{2} \rightarrow {}^{3}P_{1}$  (807 GHz) fine-structure transition and  ${}^{12}CO(7\rightarrow 6)$  (809 GHz) lines are available. The incoming beam is slit into the bands by a polarizer, and each band is sent to its own cryostat. The detectors are 64 on-chip balanced SIS mixers arranged in 8 × 8 square patterns. The beam size (FWHM) is 26" and 15" and the field coverage is 7.5' × 7.5' and 4.5' × 4.5' for the LFB and HFB respectively. The SIS mixers are expected to deliver DSB receiver temperatures < 100 K and < 200 K for the LFB and HFB respectively, which is within a factor of 5 of the quantum noise limit. The IF bandwidth is 4 to 8 GHz, so the system attains instantaneous velocity coverage of 2500 and 1500 km/sec in the LFB and HFB respectively, at velocity resolutions as high as 0.06 km/sec.

The system design is quite modular allowing for upgrades to array format and changes to frequency coverage. At first light it is expected that CHAI will have a 64-pixel array operating in the LFB. Near term planned upgrades are the addition of a 64-pixel HFB array, and the goal is to enlarge both arrays to 128-pixel formats in the future.

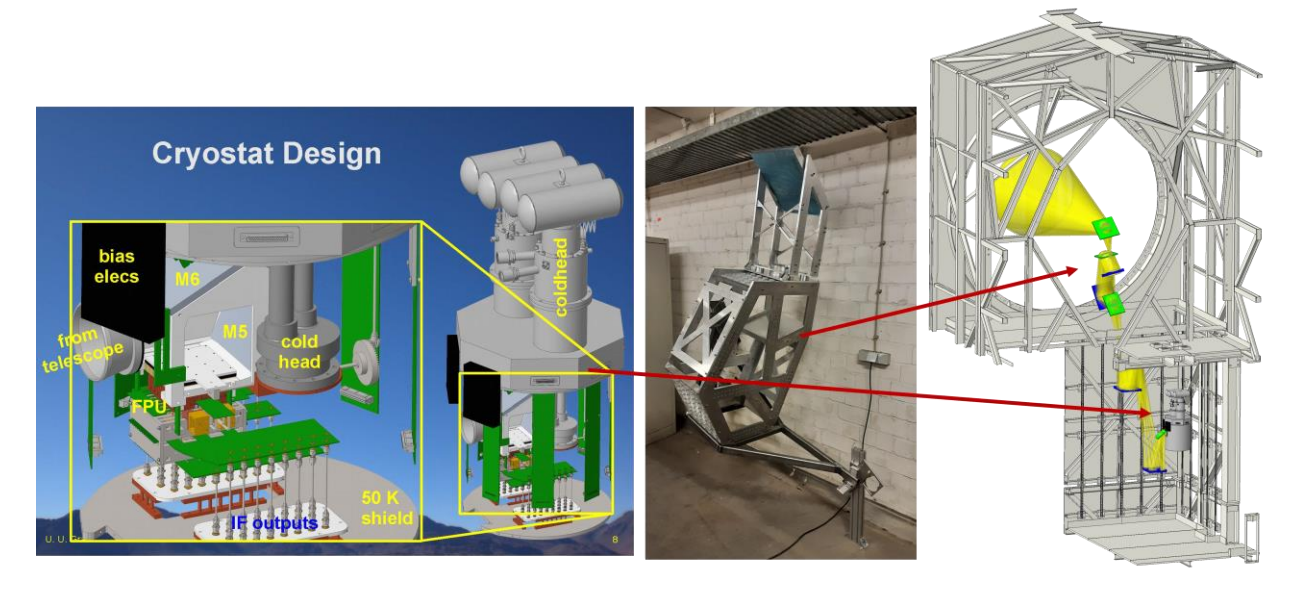


**Figure 6.** (left) Assembly drawing of the interior optical, cooling, electrical and detector system for CHAI. (center) The movable "garden gate" structure that picks off the beam in front of Prime-Cam and sends it down to CHAI in IS2. (right) Schematic of the optical system leading to CHAI. The (yellow) beam comes to a focus near the center of the elevation axis, is sent down to IS2 via the garden gate optical system, then reimaged as appropriate and polarization split for entrance into the twin cryostats of CHAI. [32].

# 4. SCIENCE IMPLEMENTATION: SURVEYS [1]

Our initial science program is designed for the first five years of operation. Within our 5-year plan, we expect the total available time for quality observations will be about 16,600 hours. About 3,300 hours will likely be used in commissioning and early science activities, and the remaining 13,300 hours will be dedicated to our "Baseline Science Program" referred to in Section 1 and described in more detail in Section 5. The time is split 75% (10,000 hours) for Prime-Cam and 25% (3,300 hours) for CHAI science.

The Prime-Cam Baseline Science Program consists of two large surveys and assorted smaller targeted observations. The large surveys include the Wide Field Survey (WFS) and the Deep Spectroscopic Survey (DSS). The WFS entails scanning a 20,000 square degree region covering declinations from -61° to +18° over the entire range of right ascension for 4000 hours total integration time on the sky. All polarimetric cameras will be operating during this survey (and likely the EoR-Spec modules as well) so that half the sky is surveyed at frequencies between 220 and 850 GHz. This survey has excellent synergy with similar surveys ongoing with ACT and planned with the Simons observatory that cover the same region at lower frequencies [33]. The WFS is designed to satisfy the wide-field science requirements for Cluster Evolution, Cosmological Foregrounds, Galaxy Evolution, Galactic Polarization, and Time Domain Astrophysics.

The DSS will use EoR-Spec to obtain deep (4000-hour total) spectroscopic surveys in 4 square degree regions of the E-COSMOS and E-CDFS deep extragalactic fields addressing our Line Intensity Mapping program. At the same time, the polarimetric cameras will be utilized to obtain deep surveys in closely aligned fields. These observations will cover deep field aspects of the Galaxy Evolution, and Time Domain Astrophysics science programs.

With Prime-Cam we also have a variety of smaller targeted observations including medium-depth observations of 100 square degrees of the GAMA field, targeted observations of nearby galaxies including the LMC and SMC, targeted observations of star formation regions of the Milky Way and cadenced observations of protostellar regions. These programs total about 2000 hours of on-source time. The Prime-Cam surveys are illustrated in Figure 7.

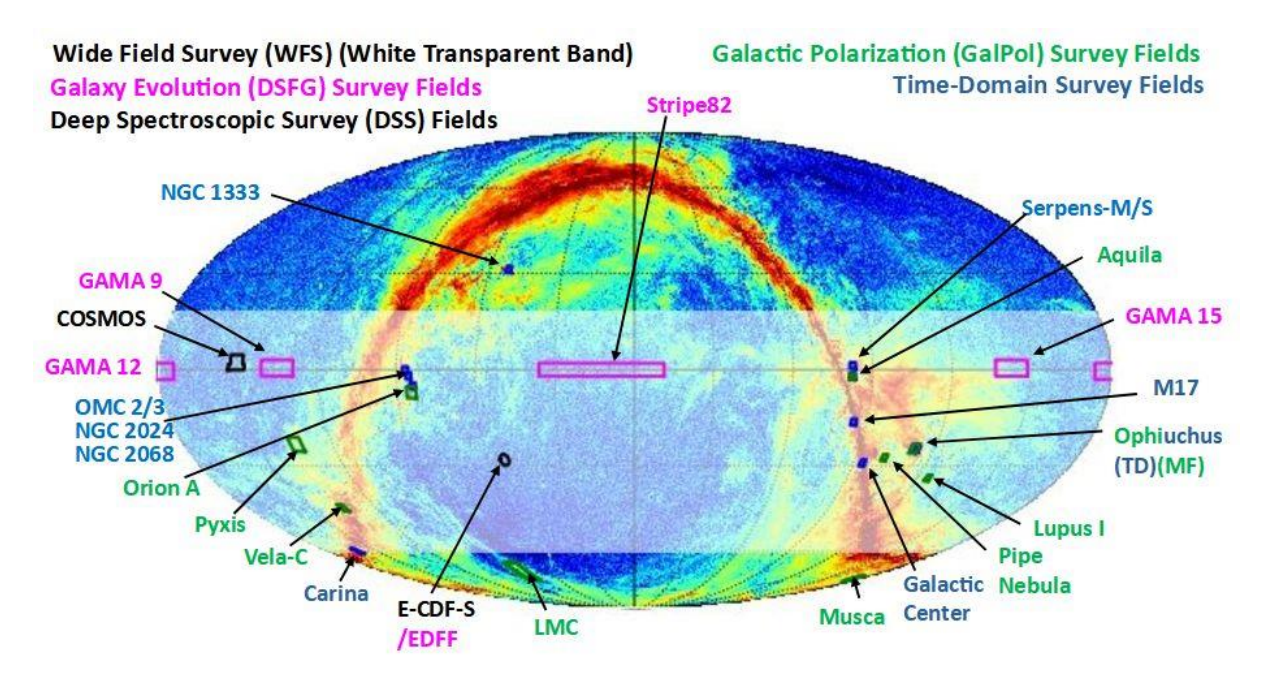


**Figure 7.** The various surveys and targets for Prime-Cam science. The WFS is the white transparent band across the sky, the DDS is the black COSMOS and E-CDFS fields. The deep 100 square degree field for Galaxy Evolution studies (Section 5.3) is outlined in magenta [1].

The CHAI Baseline Science Program has three primary components. The Galactic Mid-plane Survey covers  $110^{\circ}$  along the Galactic plane to latitudes of  $\pm 2^{\circ}$  plus cross-plane high latitude strips in the CO(4-3) and [CI] lines. This survey

entails about 53% of the CHAI time allocation. The Milky Way Out of Plane Survey include a group of nine prominent and nearby Galactic star forming molecular clouds (e.g., Taurus, Orion, Musca) that uses about 9% of their time allocation. The Nearby Galaxies Survey maps six highly resolved galaxies (SMC, LMC, NGC 253, M33, the Antennae, and M83) and uses the remaining 38% of the available time.

# 5. SCIENCE PROGRAM

# 5.1 Introduction: a brief overview of cosmic history

Our first five science themes are linked to the formation and growth of galaxies and large-scale structures in the early Universe. To put these investigations in context, we give a brief history of the Universe below.

The Universe began in a hot Big Bang about 13.8 Gyrs ago. After a very brief period of exponential growth, known as the inflationary epoch the original fireball cooled to the extent that matter (primarily protons, 4He nuclei and electrons) could exist along with, but is still thermodynamically coupled to, the hot blackbody photon radiation field. The Universe was initially far too hot for atoms to form but both the matter and radiant energy densities per unit co-moving volume cooled with the expansion. After about 370,000 years (redshift  $\sim$  1100) the Universe had cooled to  $\sim$  3000 K, at which time the free electrons combined with nuclei to form neutral hydrogen and helium. This "recombination" removed the principal photon-baryonic matter interaction – Thomson scattering of photons off electrons - so that after this point, matter and photons were thermodynamically decoupled and photons could stream freely throughout the Universe. These photons are detected today as the Cosmic Microwave Background (CMB) – an isotropic background with a blackbody temperature,  $T_{CMB} = 2.735$  K.

Until just before recombination the photon radiation field was energetically dominant, so that Thomson scattering prevented baryonic matter from collapsing to form structures. However, dark matter does not interact with photons, so that it could begin gravitationally gathering along primordial over-densities at very early times. These structures are the scaffolding for the soap bubble-like "Cosmic Web" structures that we see in the distribution of galaxies on larges scales today. Soon after recombination, baryonic matter began to gather on the dark matter structures, eventually collapsing to the first stars and accreting onto the first black holes. These energy releasing processes sent out the first photons since recombination that were capable of ionizing hydrogen, thereby beginning what is commonly called the "Epoch of Reionization", (EoR). The EoR appears to have occurred at redshifts between about 20 and 6, or about 180 to 940 Myrs after the Big Bang.

As matter accreted at over densities in the large-scale dark matter structure the first galaxies began to form. Very massive systems likely formed early at the highest over density regions. These galaxies grow by accretion of gas and the tidal disruption and accretion of stars in nearby galaxies that infall through mass segregation processes. Observations indicate that by redshifts of 6, the Universe is nearly fully ionized, and the epoch of reionization is over.

Knowledge is incomplete at present, but it appears that star formation per unit co-moving volume increases with time as more and more matter is gathered onto galaxy formation sites. The process peaks at redshifts between  $\sim 3$  and 1 at rates 10 to 30 times the star formation rates in the present-day Universe. This epoch is commonly termed "Cosmic Noon" – the peak of star formation activity over cosmic time, and the epoch in which about half of all the stars in the Universe formed. The decline in star formation following Cosmic Noon is likely driven by the growing influence of active galactic nuclei in the cores of galaxies whose outflows can both drive away accreted gas and inhibit further accretion onto the galaxy.

# 5.2 Line intensity mapping [1]

The reionization of the Universe could be due to UV light emitted by accretion onto black holes or the formation of the first stars and galaxies. It is not believed to be more likely the latter. Therefore, since the formation of galaxies is linked to the underlying dark matter distribution, by measuring the spatial scales and intensity of star formation over cosmic time, we not only learn about the formation and growth of galaxies, but we also learn about its contribution to the reionization process and can draw conclusions about the growth of structure in the Universe at redshifts between 20 and 6. This epoch is extremely challenging to investigate. Most star formation at these times is likely occurring in faint, but

very numerous low luminosity sources. These are very difficult to detect individually with any other than the largest telescope apertures, and even then, will involve long integration times. Such large apertures will necessarily have small fields of view, so that to undertake the degree-scale surveys necessary to measure the large-scale structures forming and evolving through the EoR would be prohibitively expensive. Fortunately, the fact that most of the emission arises from the multitude of faint sources opens the door to another way of pursuing this since: instead of painstakingly detecting individual sources, detect the summed emission from the faint sources in relatively large beams. The relatively large beams are delivered by smaller apertures that can have large fields of view and be dedicated to this science. This technique – observing large (degree-scale) fields with modest (arcminute-scale) beams to very low surface brightness limits is commonly known as line intensity mapping (LIM).

Carbon is the fourth most abundant element in the Universe and has an ionization potential of 11.3 eV. Carbon is therefore found in its singly ionized form ( $C^+$ ) both in the HII regions formed by early type (O/B) stars and in the neutral gas clouds from which the stars formed. The ground state ( $^2P$ ) term of the electronic configuration of  $C^+$  has two levels. The upper  $^2P_{3/2}$  level lies just 92 K above ground and is therefore easily excited by electron impacts at gas densities found in HII regions, and neutral H or  $H_2$  impacts in neutral gas clouds. The emitted 158  $\mu$ m [CII] fine-structure line is therefore an important coolant for the gas. It is also very bright (up to  $\sim$ 1% of the far-infrared luminosity of dusty star forming galaxies), and consequently an excellent tracer of star formation activity in galaxies (cf. [34],[35]). Furthermore, the [CII] line is "spectrally isolated" in the sense that the nearest line of comparable (within a factor of 10) luminosity in most star forming galaxies is the [OIII] line at 88  $\mu$ m which is at a factor of nearly two shorter wavelength. This fact makes line identification in broad surveys significantly easier. However, it will still be quite challenging, in particular due to foreground emission in CO lines from lower redshift star forming galaxies.

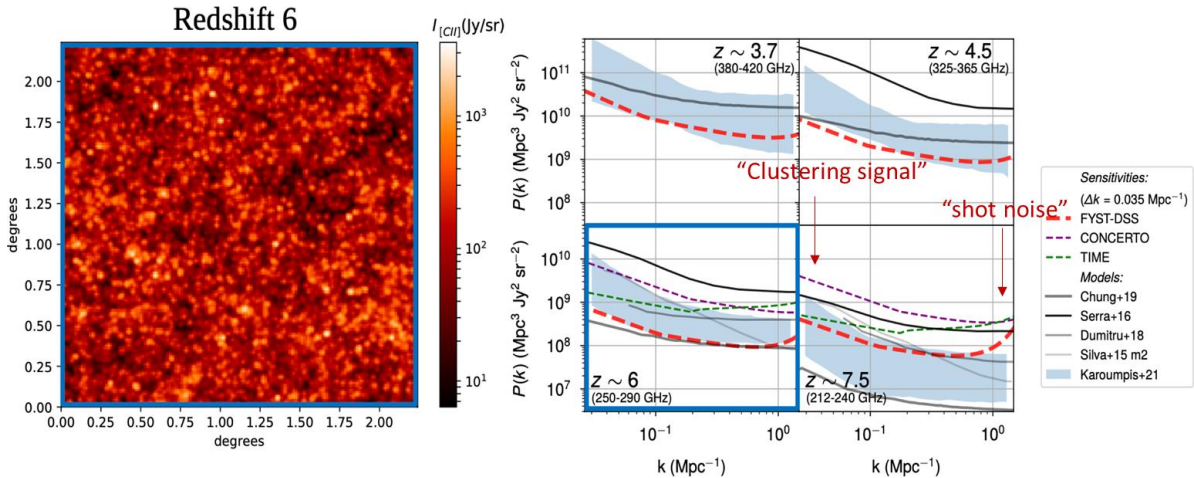


Figure 8. (left) Simulated [CII] slice at redshift 6 with frequency width 2.7 GHz wide (RP  $\sim$  100) which corresponds to a redshift slice  $\Delta z = 0.07$  at z = 6. (right) Solid lines and the blue shaded regions are predictions of the power spectrum of the [CII] line emission that reveals the topology of reionization and the [CII] luminosity function at redshifts from 3.7 to 7.5. Different models have significantly different predictions. Dashed lines show predicted sensitivities for the (ongoing) CONCERTO and CHIME surveys and predictions for EoR-Spec on FYST. EoR-Spec is equal to or better than these surveys at all redshifts and the only system planned for making these measurements at z < 5 [1].

EoR-Spec on FYST is optimized for [CII] LIM. EoR-Spec is predicted to have high optical throughput ( $\sim$  40 to 50%). The beam-size is  $\sim$  45" and the instantaneous field of view of 1.3° presented by EoR-Spec on FYST make it uniquely well suited to pursue [CII] line-based LIM science at high redshift. The beam corresponds to size-scales  $\sim$  ½ Mpc at z  $\sim$  8 – well matched to expected peaks at over densities, while the FoV corresponds to  $\sim$  24 Mpc at z  $\sim$  8 – well matched to the spatial extent of voids. The velocity resolution of 3000 km/sec matches a line-of-sight size-scale of 24 Mpc. We intend to use EoR-Spec to spectrally scan two large ( $\sim$  4 sq. degree scale) deep galaxy fields (E-COSMOS and E-CDFS) at frequencies between 210 and 420 GHz corresponding to redshifts between 8.04 and 3.5 in the [CII] line.

Figure 8 (left, from [1]) illustrates one modeled distribution of [CII] line emission over a  $2^{\circ} \times 2^{\circ}$  field at redshift 6 if we detected the field with a very low noise system. The signals will be very difficult to detect in the imaging plane with a realistic system. Fortunately, the science is derived from the size-scales of the [CII] intensity distribution which can be analyzed in the (conjugate) spatial frequency domain where each individual spatial frequency has many connections

across the field that can be joined to increase the signal to noise ratio for detection. This power spectral density signal for a variety of models is plotted in Figure 8 (right) along with the predicted detection thresholds for the EoR-Spec on FYST-DSS described here, the Concerto FTS survey planned for the APEX telescope, and the TIME survey planned for the Arizona Radio Observatory. First, we note that there is no current competition for EoR-Spec on FYST at redshifts less than 5, and FYST equals or betters the competition – by factors of up to 8 in the redshift 6 and 7.5 models. FYST should detect both the low spatial frequency, high angular extent "cluster signal" in all models for redshifts up to 7.5 and detect the high spatial frequency – point source like "shot noise" component for redshifts up to 6 for all models, and up to 7.5 for some models.

# 5.3 Galaxy evolution [1,15]

Half of star formation over cosmic time is obscured to optical observers by dust in their parent molecular clouds. The dust absorbs the starlight, heats up, and reradiates the energy in the far-infrared. Dust obscured star formation is important over cosmic time as the total power in the cosmic infrared background (CIB) is roughly the same as that in the cosmic optical background. Therefore, to trace the cosmic star formation history one needs to investigate both the optical and far-infrared backgrounds.

The infrared background at redshift < 1.5 are largely ( $\sim 80\%$ ) resolved by Spitzer and Herschel surveys into individual galaxies so that the star formation history is well understood to these redshifts. However, beyond this redshift the CIB is only partially ( $\sim 10\%$ ) resolved so that the dusty star formation history of the Universe is only very weakly described at redshifts beyond 1 which includes the epoch of galaxy assembly and the peak of star formation per unit co-moving volume at z  $\sim 1$  to 3, when most galaxies, including our own likely formed.

Prime-Cam on FYST can unveil star formation histories to redshift 5 and beyond. The 6 m FYST aperture is nearly twice that of the 3.5 m Herschel telescope. Herschel surveys were confusion limited in the submillimeter bands, and the smaller beam of FYST breaks this confusion such that FYST surveys can go about a factor of three deeper than Herschel surveys (Figure 9, left). We estimate FYST will detect about 440,000 galaxies at SNR>5 in its deep, confusion limited 100 deg<sup>2</sup> survey and therefore, the dusty cosmic star formation history will be well described out to  $z \sim 5$ . Many (>1,300) detected galaxies are likely to be at z > 5. Since our surveys are both deep, and wide they should detect the rare-beast, bright objects at very high redshifts that could be, for example, intrinsically very luminous systems such as protoclusters in formation, or highly lensed lower luminosity systems.

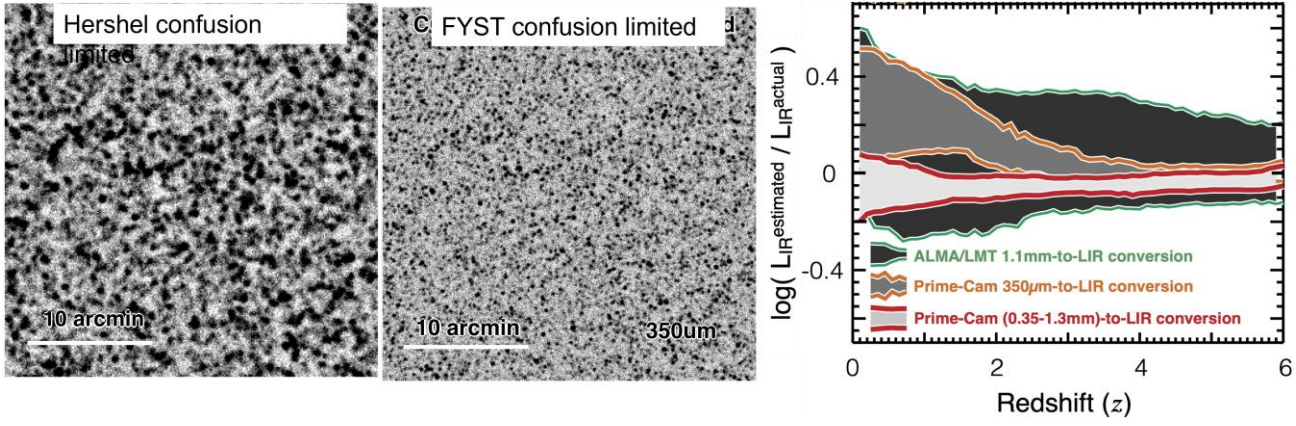


Figure 9. Simulated 850 GHz (350 μm) image of a deep field obtained with the Herschel 3.5 m telescope (left) compared with the same image as sampled by the smaller beam of the 6 m FYST telescope. FYST goes about a factor of 2.5 deeper into the confusion distinguishing many sources that could not be resolved with Herschel. (right) Ratio of source luminosity as estimated with various probes (ALMA/LMT 1.1 mm, Prime-Cam 350 μm, and Prime-Cam 0.35 to 1.3 mm) compared with the actual luminosity modeled for dusty star forming galaxies as redshifts up to 6. The single-wavelength estimates are much inferior to the multi-wavelength estimates. At redshift ~ 3, single band 1.1 mm estimates have errors ~  $\pm 0.2$  dex with large zero bias, the errors for single band 350 μm work have errors ~  $\pm 0.12$  dex with significant bias, while the multi-wavelength estimates have errors ~  $\pm 0.05$  dex with significantly lower bias [1].

The 850 GHz (350  $\mu$ m) instrument module is critical to the Prime-Cam discovery space and interpretation. The thermal dust spectrum for dusty star forming galaxies typically peaks at rest wavelengths between 50 and 100  $\mu$ m. Measuring this peak flux density yields good estimates for the source luminosity if the redshift is known. The 850 GHz camera can

therefore provide good luminosity estimates for sources between  $z\sim2.5$  to 6. The lower frequency modules on Prime-Cam greatly improve the scientific yield by sampling source dust spectral energy distributions so dust peaks may be found, yielding statistical redshifts and therefore statistical source luminosities *without a priori* knowledge of redshift. The utility of multiple frequency sampling is illustrated in Figure 9 (right). Here we show that within a statistical single wavelength sample, for instance a 1.1 mm wavelength survey conducted with ALMA or the LMT, or just a 350  $\mu$ m survey with Prime-Cam on FYST will have much larger error estimates and much more significant bias from zero over all redshifts (1.1 mm survey) or at z<4 (350  $\mu$ m survey). The multiband surveys available with Prime-Cam on FYST yield much better estimates of source luminosity, with near zero bias from the local Universe to redshift beyond 6.

# 5.4 Probing cluster evolution with the Sunyaev-Zel'dovich effect. [1]

Galaxy clusters are the most massive gravitationally bound structures in the Universe. The very deep gravitational well in the cores of clusters ensure that any gas has temperatures of the order millions of K. The electrons in this hot ionized gas will act as a scattering screen in front of the background CMB radiation altering its spectrum through inverse Compton scattering: "cold" photons boosted by "hot" electrons. This process is called the Sunyaev-Zel'dovich (SZ) effect and the resultant shift in the CMB spectrum can probe fundamental properties of the Universe as well as the astrophysics of clusters including star formation and AGN feedback.

The SZ effect has three important components that we can probe with Prime-Cam on FYST. These components are entangled in the spectrum, but with its access to high frequency observations, observations with Prime-Cam on FYST can de-tangle the effects so that the rich physics associated with the effects can be unveiled.

The thermal SZ (tSZ) is dominant. It involves simple promotion of photons with frequencies below the 220 GHz null to higher frequencies. This has a characteristic shape (Figure 10) and the amplitude of this effect is a measure of the total thermal energy in the cluster. The kinetic SA (kSZ) effect arises when the cluster gas velocity is in motion with respect to the CMB – a Doppler shift when the cluster has a peculiar velocity with respect to the Hubble flow. The amplitude of the kSZ spectrum is proportional to the line-of-sight electron momentum. A third, weaker effect is the relativistic SZ (rSZ) effect that is a measure of the mean temperature of the scattering electrons. The magnitude of each effect is governed by the mass of the cluster, the strength of AGN activity and the motion of matter on large scales leading to constraints on models of gravity, dark energy, and fundamental particle physics as well as cluster astrophysics.

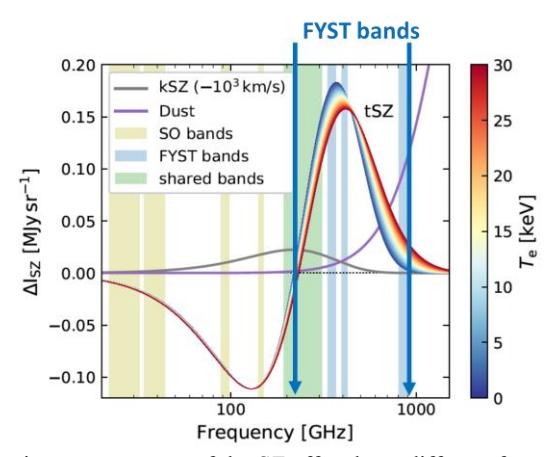


**Figure 10.** SZ effects. The various components of the SZ effect have different frequency spectra that manifest themselves most strongly in the higher frequency bands. Therefore, observing clusters the Prime-Cam/FYST bands enable detangling the processes so that cluster properties and their relationship to both fundamental physics and the astrophysics of clusters may be derived [1].

The numbers of galaxy clusters identified through the tSZ effect is in the thousands enabling first studies of the growth of structure based on number counts and their angular correlations. However, these constraints are limited by the individual cluster gas properties including pressure, temperature and density profiles that can be derived from the combination of tSZ, kSZ, and rSZ measurements. The physical properties of the cluster gas are also important for studies of the effects of AGN activity on gas heating and the AGN-star formation feedback process for cluster galaxies.

Cluster studies based solely on frequencies less than about 220 GHz are hard pressed to separate the contributions of the various SZ effects to the observed spectrum. However, the higher frequency (220 to 850 GHz) measurements that we will obtain with Prime-Cam make a very difficult problem tractable (Figure 10). Warm dust emission can be important at SZ frequencies so that measuring the higher frequencies with Prime-Cam dust contamination can be removed for improved SZ measurements. The presence of warm dust is also a key element of cluster astrophysical studies.

#### 5.5 Galactic ecology

# 5.5.1 Thermal dust emission and magnetic fields with Prime-Cam [1]

Interstellar dust makes up less than 1% of the mass of the interstellar medium (ISM) but has profound effects on astrophysics. With a typical size scale of  $0.1~\mu m$ , dust interacts very strongly with visible light limiting our view of the stars in the Milky Way and other star forming galaxies. These effects are so strong that since stars are formed in dusty molecular cloud cores it quite challenging if not impossible to view the final stages of star formation and the youngest stars in the visible band. The absorbed optical energy heats the dust to a few tens of Kelvins so that the dust then reradiates the optical power in the far-infrared to submillimeter bands. As pointed out in Section 5.3~a above, half the starlight power every emitted is absorbed by dust and reradiated in these bands, so that dust is an important ingredient of the interstellar medium over the history of star formation in the Universe.

Non-spherical dust grains in the ISM will align with interstellar magnetic fields so that thermal dust emission will carry a linear polarization signal. The polarization signal direction is indicative of the field strength in the plane of the sky and the polarization light fraction reflects both intrinsic dust grain properties and the 3-D properties of the interstellar magnetic fields. Prime-Cam will measure polarization in all of its camera modes. During the 20,000 square degree 4000 hours WFS much of the Galactic Plane will be observed (see Figure 7 above) and we will learn much about the large-scale magnetic field structure in the Galaxy at the same time we are tracing ISM structures in dust thermal emission at spatial resolutions between 60" (at 220 GHz) and 15" (at 850 GHz) corresponding to about 8000 and 2000 AU respectively at the nearby molecular clouds (e.g. Taurus at 140 pc). These large-scale surveys tie into properties of interstellar turbulence and magnetic field effects on cloud structure and star formation over a broad range of environments.

By observing translucent clouds, we can measure dust extinction, dust emission, and magnetic field directions which reflects grain alignment. The combined parameters are sensitive to grain composition: hydrocarbon rich grains reach higher temperatures and have less polarization in their emission than silicate grains. Therefore, the dust spectrum and polarization properties reflect not only magnetic fields, but also grain composition. Recent studies have shown that grain composition may not as simple as a silicate/carbonaceous dichotomy. New models have been proposed for grain composition, the difference between models arising most strongly with the degree of polarization as a function of frequency in the higher frequency Prime-Cam bands. These effects can be important for CMB studies (Section 5.6).

# 5.5.2 Velocity-resolved submillimeter line emission with CHAI

The CHAI spectrometer is designed for large field mapping of the astrophysically important [CI]  ${}^{3}P_{1} \rightarrow {}^{3}P_{0}$  (492 GHz) and [CI]  ${}^{3}P_{2} \rightarrow {}^{3}P_{1}$  (807 GHz) fine-structure lines and the mid-J CO(7-6) 806 GHz and CO(4-3) 460 GHz rotational lines. The lines are important tracers of molecular cloud structure and gas excitation: the [CI] line ratio is predominantly a tracer of gas temperature and column density, while the CO line ratio is a primarily a measure of gas pressure. These lines can all be strongly emitted from the warm dense photodissociation regions (PDRs) on the surfaces of molecular clouds exposed to the ionizing radiation of nearby stars. In this case they trace PDR structure, heating and cooling, gas density and temperature. Within the PDR CO is photodissociated, but due to self-shielding, about half the hydrogen gas in the PDR will be in molecular form. CO is the preferred tracer of molecular gas content in galaxies, so that these CO-free molecular hydrogen regions have come to be called "CO-dark molecular gas". Since the PDR structure is dominated by extinction of far-UV photons by dust, the CO dark region of molecular clouds can be dominant in low metallicity systems where dust extinction, which is likely to be proportional to metallicity, is proportionally smaller. The [CI] line is an excellent tracer of PDR structure in these types of molecular clouds so CHAI dark-gas studies will highlight low metallicity systems such as the LMC and SMC. The mid-J CO lines trace the warmer molecular gas at the CO surface of molecular clouds but are also sensitive to shocks and therefore good tracers of turbulence and its relationship to star formation in molecular clouds (cf. [36], [37]).

CHAI will also map a  $110^{\circ} \times 4^{\circ}$  path along the Galaxy from longitudes of 80 degrees through the Galactic Center and on to 330 degrees (Figure 11). The combined [CI] and CO line maps will trace the accumulation and flows of gas into cores and young stars. With a 15" beam at 800 GHz the spatial scales covered in such maps are 25,000:1. In the nearest molecular clouds the 15" beam subtends about 2000 AU.

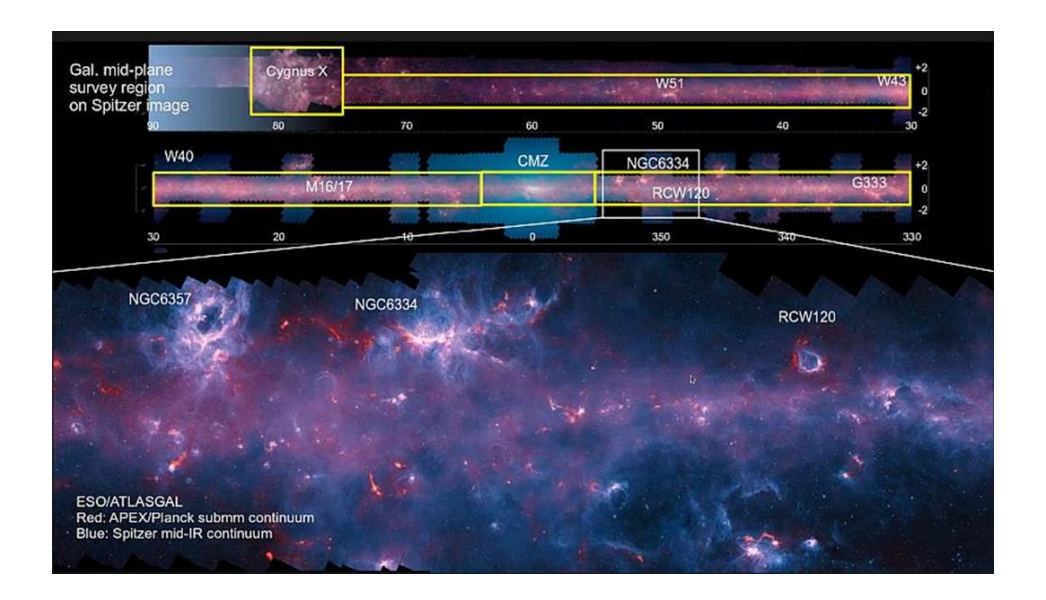
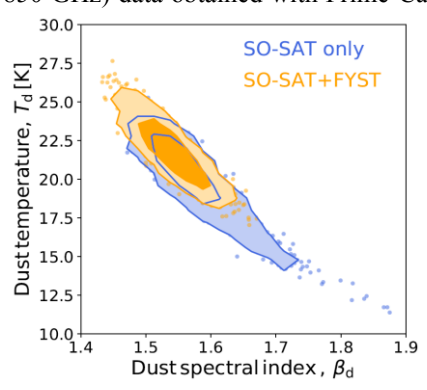


Figure 11. Galactic science with CHAI. In addition to focused mapping of Galactic HII regions and nearby Galaxies, CHAI will undertake a map of the Galactic plane covering a longitude from  $80^{\circ}$  through the Galactic Center to  $330^{\circ}$  and  $\pm 2^{\circ}$  in latitude (outlined in yellow). The map samples a wide variety of environments from giant HII regions to small protostellar cores. The spectrally resolved lines will enable studies of gas flow from large to small scales and Galactic structure as traced by neutral gas lines.

# 5.6 Dusty foregrounds and the search for gravitational waves

Grain composition and the polarization of its thermal emission is not only important for ISM studies – it is a critical input for detection of primordial gravitational waves (or tensor perturbations) through CMB polarization studies. As discussed in [1] the Galactic foreground polarization must be very accurately described and subtracted off from cosmological polarization measurements to detect the small, but non-zero tensor-to-scalar ratio, r that is expected in most models for primordial inflation-induced gravity waves. Knowledge of the foreground Galactic dust spectral emissivity index,  $\beta_d$  and temperature,  $T_d$  are key inputs for foreground subtraction. Figure 12 shows that the index and the dust temperature are weakly constrained with just the lower frequency (< 280 GHz) bands planned in Simons Observatory (SO) observations. The constraints become much better when including the high frequency (350, 410, and 850 GHz) data obtained with Prime-Cam. With a poorly defined dust parameters, there is residual bias in the expected



tensor-to-scalar ratio that is of the same order as the expected signal:  $r_{SO-SAT} = (1.3 \pm 2.8) \times 10^{-3}$ . By combining the high frequency Prime-Cam/FYST data with SO-SAT, the bias goes essentially to zero:  $r_{SO-SAT+FYST} = (0.2 \pm 2.7) \times 10^{-3}$ .

**Figure 12.** The best fit dust parameters  $\beta_d$  and  $T_d$  are much better determined by combining the high frequency (350, 410, and 850 GHz) band data from FYST with the lower frequency data of the Simons observatory (SO-SAT). The determination of the dust parameters will significantly reduce the residual bias in determining the tensor-to-scalar ratio. r [1].

# 6. STATUS AND SCHEDULE [3]

Essentially all elements of the CCAT-prime project outlined in this paper are either in an advanced design phase, under construction or completed.

#### **6.1 Site**

In preparation for the construction of the FYST telescope and University of Tokyo Atacama Observatory (TAO) 6.5 m mid-IR telescope [38], the road to the FYST and the TAO sites has been upgraded to eliminate difficult switchbacks and steep, or dangerous climbs (Figure 13). The fiber and power cables installation is in progress, and the CCAT/TAO service area is prepared near the ALMA road. Power will be provided with diesel generators at the service area. The 5600 m elevation site on Cerro Chajnantor is now leveled, the foundation hole for the FYST telescope is excavated and the first layer of concrete is in place at the bottom of this excavation (Figure 14). It is expected that the final layers of the foundation will be poured in the 3<sup>rd</sup> quarter of 2022. Under routine operations, the telescope will be remotely operated [39], observing 12 to 18 hours/day during the prime season from mid-March to mid-December.

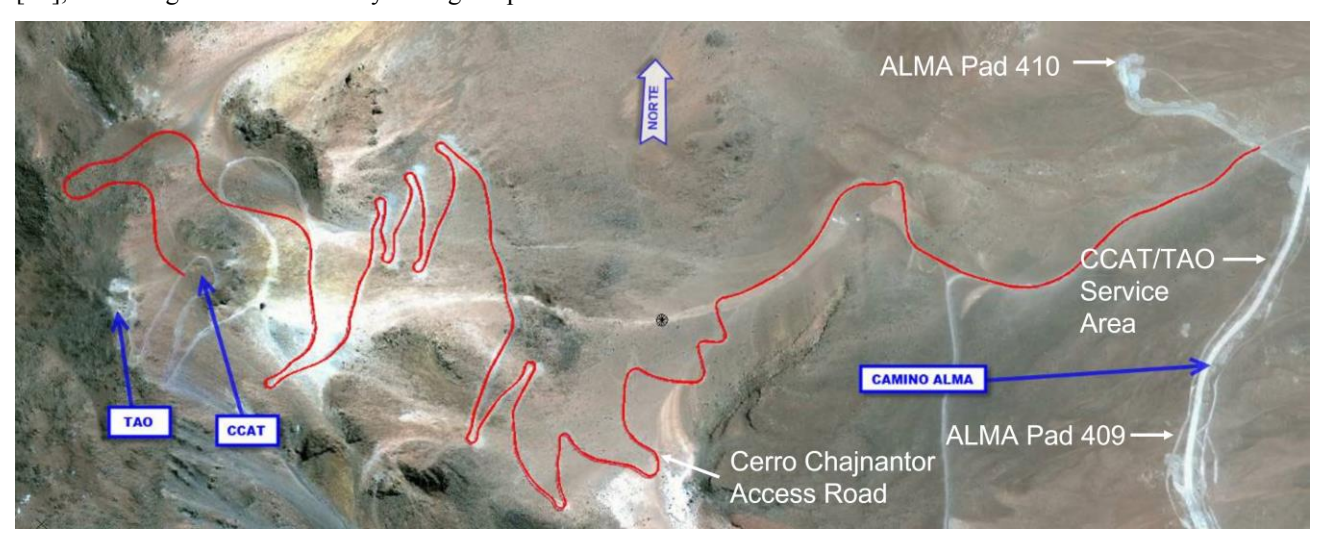


Figure 13. Site map. The red curved line is the upgraded road to the FYST and TAO sites from the ALMA road (right, white curves).



**Figure 14**. (left) Service area view from Cerro Chajnantor. (center) Trenching (and protective bricks) for power/data cables. (right) FYST site is leveled and the telescope foundation pour has begun.

# 6.2 Telescope and mount

Telescope mirror panels for both the primary and secondary are complete and have come in at better than specifications (Figure 15). The carbon fiber based backing structure design is complete, but construction is behind schedule due to material sourcing issues.

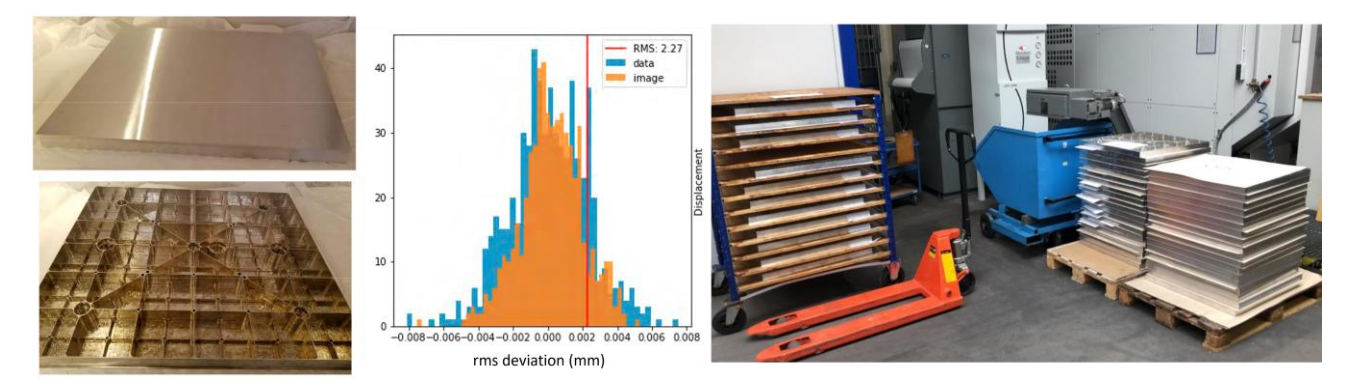


**Figure 15.** (left) Front side (top) of a completed mirror panel. The panels are approximately 0.6 m on a side. The mirror panels are made of highly light weighted aluminum (bottom). (center) distribution of rms wavefront errors for the mirror panels. The mean is well below the required 2.27 µm rms wavefront error. (right) Panels being stored.

The components of the telescope mount base – the precast concrete foundation cone, and the overlying metal support cone containing the azimuth ring etc. are now complete (Figure 16). The precast concrete foundation cone lies below ground level and will be transported to the site then filleted with concrete to form the foundation base to which the metal support cone attaches.







**Figure 16.** (left) Concrete support cone elements precast in Chile. There are 13 elements totaling 324 tons in weight. (center) Support pad prepared in Wessel, Germany, with a support ring in the background. This is the foundation for a trial assembly of the full telescope in Germany. (right) Support ring bolted onto the pad. The azimuth bearing is on the top of this ring.

Most of the structural elements of the telescope mount are now complete or awaiting painting including both yoke arms, the yoke traverse, and the support cone. The instrument spaces are in progress (Figure 17).



**Figure 17.** (left) Structure design of the FYST. The left and right yoke arms (light green and light red) and the yoke traverse (green) are manufactured and awaiting test fit assembly in Wessel (right).

# 6.3 Instruments

The Prime-Cam cryostat is fully designed and being manufactured at Redline Chambers, Inc. (Figure 18). Delivery of the completed, vacuum-tested cryostat is expected early fall 2022.

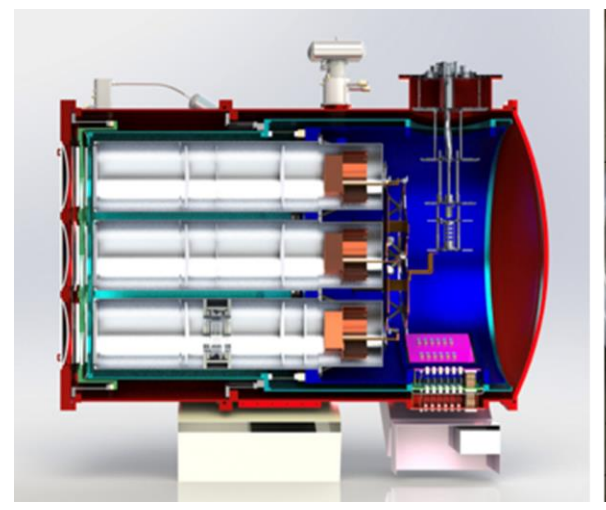




**Figure 18.** (left) Cutaway of the Prime-Cam cryostat design showing instrument modules (white) the ADR, pressure vessel and thermal shields. (right) Front end of the cryostat showing the openings for the seven instrument module windows. Mod-Cam is complete and will be used for testing when the first instrument module (280 GHz) is completed.

Optical designs for all the instrument modules are essentially complete, detector array wiring harnesses and support/interface structures are designed - several of these are manufactured and undergoing laboratory testing. The first instrument module (for the 280 GHz system) is designed and in manufacture, lenses have been ordered for this module, and its first array from NIST is undergoing laboratory testing at Cornell [38]. We plan to read-out our arrays with a Radio Frequency System RFSoC based system [11].

#### 6.4 Schedule

The schedule for the telescope is the following:

- 2022-Q3: Fabrication complete
- 2023-Q2: Pre-Assembly and factory testing at Wessel complete
- 2023-Q3: Transport to Chile
- 2024-Q1: Final assembly on Cerro Chajnantor
- 2024-Q2: Final acceptance leading to first light

The schedule for Prime-Cam and Mod-Cam that follows is highly dependent on the qualification schedules for the various instrument modules, as well as the assembly and test schedule for Prime-Cam.

Our Goal schedule is shipping Prime-Cam down to Chile in Q4 of 2023 with three modules installed in time for observations on FYST in 2024. The likely modules are the 280 GHz, 350 GHz and an EoR spec modules. Then, in late 2024 the 850 GHz instrument module would be shipped down and installed in Prime-Cam for observations starting in 2025.

If Prime-Cam is not ready in Q4 of 2023 we will ship Mod-Cam down to Chile with the 280 GHz instrument module for observations in 2024. In Q4 of 2024 Prime-Cam ships down to FYST with the 350 GHz, 850 GHz and one (or possibly two) EoR-Spec modules for observations in 2025.

In both cases, we envision other modules arriving in Q4 of 2025 for observations beginning in 2026.

CHAI will be shipped to Chile in Q4 of 2023 with a 64-pixel LFB array for first light in 2024. The 64-pixel HFB array will be delivered one year later, for 2025 observations.

#### **ACKNOWLEDGEMENTS**

Scores of people have contributed to the work reviewed within this document, and as part of the CCAT-prime Collaboration. Most, if not all, of the contributors can be found as co-authors on the referenced CCAT-prime related papers.

The CCAT-prime project, FYST and Prime-Cam instrument have been supported by generous contributions from the Fred M. Young, Jr. Charitable Trust, Cornell University, and the Canada Foundation for Innovation and the Provinces of Ontario, Alberta, and British Columbia. The construction of the FYST telescope was supported by the Grosgeräte-Programm of the German Science Foundation (Deutsche Forschungsgemeinschaft, DFG) under grant INST 216/733-1 FUGG, as well as funding from Universität zu Köln, Universität Bonn and the Max Planck Institut für Astrophysik, Garching. The construction of EoR-Spec is supported by NSF grant AST-2009767. The construction of the 350 GHz instrument module for Prime-Cam is supported by NSF grant AST-2117631. The CHAI instrument is supported by DFG grant CRC 956/3, project ID 184018867 as well as funding from Universität zu Köln.

#### REFERENCES

- [1] CCAT-Prime collaboration, Aravena, M., Austermann, J. E., Basu, K., Battaglia, N., Beringue, B., Bertoldi, F., Bigiel, F., Bond, J. R., Breysse, P. C., Broughton, C., Bustos, R., Chapman, S. C., Charmetant, M., Choi, S. K., Chung, D. T., Clark, S. E., Cothard, N. F., Crites, A. T., Dev, A., Douglas, K., Duell, C. J., Ebina, H., Erler, J., Fich, M., Fissel, L. M., Foreman, S., Gao, J., Garc'ia, P., Giovanelli, R., Haynes, M. P., Hensley, B., Herter, T., Higgins, R., Huber, Z., Hubmayr, J., Johnstone, D., Karoumpis, C., Keating, L. C., Komatsu, E., Li, Y., Magnelli, B., Matthews, B. C., Meerburg, P. D., Meyers, J., Muralidhara, V., Murray, N. W., Niemack, M. D., Nikola, T., Okada, Y., Riechers, D. A., Rosolowsky, E., Roy, A., Sadavoy, S. I., Schaaf, R., Schilke, P., Scott, D., Simon, R., Sinclair, A. K., Sivakoff, G. R., Stacey, G. J., Stutz, A. M., Stutzki, J., Tahani, M., Thanjavur, K., Timmermann, R. A., Ullom, J. N., van Engelen, A., Vavagiakis, E. M., Vissers, M. R., Wheeler, J. D., White, S. D. M., Zhu, Y., and Zou, B., "CCAT-prime Collaboration: Science Goals and Forecasts with Prime-Cam on the Fred Young Submillimeter Telescope," arXiv e-prints, arXiv:2107.10364 (July 2021).
- [2] Parshley, S. C., Niemack, M., Hills, R., Dicker, S. R., Dünner, R., Erler, J., Gallardo, P. A., Gudmundsson, J. E., Herter, T., Koopman, B. J., Limon, M., Matsuda, F. T., Mauskopf, P., Riechers, D. A., Stacey, G. J., and Vavagiakis, E. M., "The optical design of the six-meter CCAT-prime and Simons Observatory telescopes," in [Ground-based and Airborne Telescopes VII], Marshall, H. K. and Spyromilio, J., eds., Society of Photo-Optical Instrumentation Engineers (SPIE) Conference Series 10700, 1070041 (July 2018).
- [3] Parshley, Stephen C. et al. "CCAT-prime: the Fred Young Submillimeter Telescope (FYST) final design and fabrication" in [Millimeter, Submillimeter, and Far-Infrared Detectors and Instrumentation for Astronomy XI], Society of Photo-Optical Instrumentation Engineers (SPIE) Conference Series 12190-4 (July 2022).
- [4] C. Dragone, "Offset multireflector antennas with perfect pattern symmetry and polarization discrimination," AT&T Technical Journal 57, 2663–2684 (1978).
- [5] Niemack, M. D., "Designs for a large-aperture telescope to map the CMB 10× faster," *Applied Optics* **55**, 1686 (Mar. 2016).
- [6] Vavagiakis, E. M., Ahmed, Z., Ali, A., Basu, K., Battaglia, N., Bertoldi, F., Bond, R., Bustos, R., Chapman, S. C., Chung, D., Coppi, G., Cothard, N. F., Dicker, S., Duell, C. J., Duff, S. M., Erler, J., Fich, M., Galitzki, N., Gallardo, P. A., Henderson, S. W., Herter, T. L., Hilton, G., Hubmayr, J., Irwin, K. D., Koopman, B. J., McMahon, J., Murray, N., Niemack, M. D., Nikola, T., Nolta, M., Orlowski-Scherer, J., Parshley, S. C., Riechers, D. A., Rossi, K., Scott, D., Sierra, C., Silva-Feaver, M., Simon, S. M., Stacey, G. J., Stevens, J. R., Ullom, J. N., Vissers, M. R., Walker, S., Wollack, E. J., Xu, Z., and Zhu, N., "Prime-Cam: a first- light instrument for the CCAT-prime telescope," in [Millimeter, Submillimeter, and Far-Infrared Detectors and Instrumentation for Astronomy IX],

- Zmuidzinas, J. and Gao, J.-R., eds., Society of Photo-Optical Instrumentation Engineers (SPIE) Conference Series 10708, 107081U (July 2018).
- [7] Choi, S. K., Austermann, J., Basu, K., Battaglia, N., Bertoldi, F., Chung, D. T., Cothard, N. F., Duff, S., Duell, C. J., Gallardo, P. A., Gao, J., Herter, T., Hubmayr, J., Niemack, M. D., Nikola, T., Riechers, D., Rossi, K., Stacey, G. J., Stevens, J. R., Vavagiakis, E. M., Vissers, M., and Walker, S., "Sensitivity of the Prime-Cam Instrument on the CCAT-Prime Telescope," *Journal of Low Temperature Physics* 199, 1089–1097 (Mar. 2020).
- [8] Vissers, Michael R. et al., "Hybrid TiN-Al MKIDs" in [Millimeter, Submillimeter, and Far-Infrared Detectors and Instrumentation for Astronomy XI], Society of Photo-Optical Instrumentation Engineers (SPIE) Conference Series 12190-4 (July 2022).
- [9] Duell, Cody J. et al. "Superconducting resonators & kinetic inductance detectors: a practical introduction using Jupyter notebooks" in [Millimeter, Submillimeter, and Far-Infrared Detectors and Instrumentation for Astronomy XI], Society of Photo-Optical Instrumentation Engineers (SPIE) Conference Series 12190-4 (July 2022).
- [10] Li, Yaqiong et al., "CCAT-prime: the Design of the Epoch of Reionization Spectrometer Detector Arrays," in [Millimeter, Submillimeter, and Far-Infrared Detectors and Instrumentation for Astronomy XI], Society of Photo-Optical Instrumentation Engineers (SPIE) Conference Series 12190-154 (July 2022).
- [11] Sinclair, A. et al., "CCAT-prime: RFSoC based readout for frequency multiplexed kinetic inductance detectors," in [Millimeter, Submillimeter, and Far-Infrared Detectors and Instrumentation for Astronomy XI], Society of Photo-Optical Instrumentation Engineers (SPIE) Conference Series 12190-66 (July 2022).
- [12] Li, Yaqiong et al. "CCAT-prime: Prototype Submillimeter-wave Aluminum Kinetic Inductance Detectors Fabricated with Electron-beam Lithography" in [Millimeter, Submillimeter, and Far-Infrared Detectors and Instrumentation for Astronomy XI], Society of Photo-Optical Instrumentation Engineers (SPIE) Conference Series 12190-66 (July 2022).
- [13] Hubmayr, J. et al. "Photon-noise limited sensitivity in titanium nitride kinetic inductance detectors", Applied Physics Letters, 106, 073505 (2015).
- [14] Choi, S.K. et al., "CCAT-prime: characterization of the 280 GHz MKID array for Prime-Cam" in [Millimeter, Submillimeter, and Far-Infrared Detectors and Instrumentation for Astronomy XI], Society of Photo-Optical Instrumentation Engineers (SPIE) Conference Series 12190-157 (July 2022).
- [15] Calvo, M. et al. "The NIKA2 Instrument, A Dual-Band Kilopixel KID Array for Millimetric Astronomy" Journal of Low Temperature Physics, 184, 86 (2016)
- [16] Chapman, Scott C. et al., "CCAT-prime: The 850GHz camera for Prime-Cam on FYST" in [Millimeter, Submillimeter, and Far-Infrared Detectors and Instrumentation for Astronomy XI], Society of Photo-Optical Instrumentation Engineers (SPIE) Conference Series 12190-4 (July 2022).
- [17] Huber, Anthony I. et al. "CCAT-prime: optical and cryogenic design of the 850 GHz module for Prime-Cam" in [Millimeter, Submillimeter, and Far-Infrared Detectors and Instrumentation for Astronomy XI], Society of Photo-Optical Instrumentation Engineers (SPIE) Conference Series 12190-4 (July 2022).
- [18] Nikola, Thomas et al. "CCAT-prime: The Epoch of Reionization Spectrometer for Prime-Cam on FYST" in [Millimeter, Submillimeter, and Far-Infrared Detectors and Instrumentation for Astronomy XI], Society of Photo-Optical Instrumentation Engineers (SPIE) Conference Series 12190-4 (July 2022).
- [19] Crites, Abbe et al. "TIME, the Tomographic Ionized Carbon Intensity Mapping Experiment: an update on design, characterization, and data from the 2022 commissioning observations" in [Millimeter, Submillimeter, and Far-Infrared Detectors and Instrumentation for Astronomy XI], Society of Photo-Optical Instrumentation Engineers (SPIE) Conference Series 12190-4 (July 2022).
- [20] Catalano, A., et al. "CONCERTO at APEX: Installation and first phase of on-sky commissioning" EPJWC.25700010C (2022)
- [21] Shirokoff, Eric et al. "First demonstration of the SuperSpec on-chip spectrometer at the Large Millimeter Telescope" in [Millimeter, Submillimeter, and Far-Infrared Detectors and Instrumentation for Astronomy XI], Society of Photo-Optical Instrumentation Engineers (SPIE) Conference Series 12190-4 (July 2022).
- [22] Buijtendorp, Bruno et al. "DESHIMA 2.0: Laboratory demonstration of the ultra-wideband integrated superconducting spectrometer" in [Millimeter, Submillimeter, and Far-Infrared Detectors and Instrumentation for Astronomy XI], Society of Photo-Optical Instrumentation Engineers (SPIE) Conference Series 12190-4 (July 2022).
- [23] Poglitsch, A; Beeman, J. W.; Geis, N.; Genzel, R.; Haggerty, M.; Haller, E. E.; Jackson, J.; Rumitz, M.; Stacey, G. J.; Townes, C. H. "The MPE/UCB far-infrared imaging Fabry-Perot interferometer (FIFI)", International Journal of Infrared and Millimeter Waves, 12, Issue 8, 859-884 (1991)

- [24] Latvakoski, H. M.; Stacey, G. J.; Gull, G. E.; Hayward, T. L. "Kuiper Widefield Infrared Camera Far-Infrared Imaging of the Galactic Center: The Circumnuclear Disk Revealed", ApJ 511, 761L (1999)
- [25] Bradford, C. Matt; Stacey, Gordon J.; Swain, Mark R.; Nikola, Thomas; Bolatto, Alberto D.; Jackson, James M.; Savage, Maureen L.; Davidson, Jacqueline A.; Ade, Peter A. R. "SPIFI: a direct-detection imaging spectrometer for submillimeter wavelengths" Applied Optics, 41, 2561-2574 (2002)
- [26] Douthit, Greg; Stacey, Gordon; Nikola, Thomas; Henderson, Chuck; Gull, George; Rossi, Kayla; Kutryrev, Alexander; Moseley, Samuel "Development of the Fabry-Perot interferometers for the HIRMES spectrometer on SOFIA" Proceedings of the SPIE, Volume 10708, id. 107081P 13 pp. (2018).
- [27] Cothard, N. F., Choi, S. K., Duell, C. J., Herter, T., Hubmayr, J., McMahon, J., Niemack, M. D., Nikola, T., Sierra, C., Stacey, G. J., Vavagiakis, E. M., Wollack, E. J., and Zou, B., "The Design of the CCAT-prime Epoch of Reionization Spectrometer Instrument," *Journal of Low Temperature Physics* 199, 898–907 (Jan. 2020).
- [28] Zou, B. et al., "The design and characterization of the silicon mirrors for the Fabry-Perot interferometer in the Epoch of Reionization Spectrometer," in [Millimeter, Submillimeter, and Far-Infrared Detectors and Instrumentation for Astronomy XI], Society of Photo-Optical Instrumentation Engineers (SPIE) Conference Series 12190-148 (July 2022).
- [29] Huber, Z. B., Niemack, M. D., et al., "Prime-Cam: the optical design for the Epoch of Reionization spectrometer," in [Millimeter, Submillimeter, and Far-Infrared Detectors and Instrumentation for Astronomy XI], Society of Photo-Optical Instrumentation Engineers (SPIE) Conference Series 12190-157 (July 2022).
- [30] Vavagiakis, E. M. aet al., "CCAT-prime: Design and testing of the Mod-Cam receiver and 280 GHz MKID instrument module," in [Millimeter, Submillimeter, and Far-Infrared Detectors and Instrumentation for Astronomy XI], Society of Photo-Optical Instrumentation Engineers (SPIE) Conference Series 12190-4 (July 2022).
- [31] Stacey, G. J. 2011, IEEE Transactions on Terahertz Science and Technology, 1, 241
- [32] Graf, U. U., Honingh, N., Barrueto, I., et al., "CHAI, the CCAT-prime Heterodyne Array Instrument," 30th International Symposium on Space Terahertz Technology 30, 77 (2019).
- [33] Stevens, Jason R., et al. "Designs for next generation CMB survey strategies from Chile" in SPIE Astronomical Telescopes + Instrumentation Proceedings Volume 10708, Millimeter, Submillimeter, and Far-Infrared Detectors and Instrumentation for Astronomy IX; 1070841S (July 2018).
- [34] Stacey, G. J., Geis, N., Genzel, R., Lugten, J. B., Poglitsch, A., Sternberg, A., and Townes, C. H., "The 158 Micron [C II] Line: A Measure of Global Star Formation Activity in Galaxies," *ApJ* 373, 423 (June 1991).
- [35] Stacey, G. J., Hailey-Dunsheath, S., Ferkinhoff, C., Nikola, T., Parshley, S. C., Benford, D. J., Staguhn, J. G., and Fiolet, N., "A 158 μm [C II] Line Survey of Galaxies at z ~1-2: An Indicator of Star Formation in the Early Universe," *ApJ* 724, 957–974 (Dec. 2010).
- [36] Okada, Yoko; Güsten, Rolf; Requena-Torres, Miguel Angel; Röllig, Markus; Stutzki, Jürgen; Graf, Urs Ulrich; Hughes, Annie "Velocity profiles of [CII], [CI], CO, and [OI] and physical conditions in four star-forming regions in the Large Magellanic Cloud" *A&A* 621, A62 27 pp (Jan. 2019).
- [37] Beuther, H.; Ragan, S. E.; Ossenkopf, V.; Glover, S.; Henning, Th.; Linz, H.; Nielbock, M.; Krause, O.; Stutzki, J.; Schilke, P.; Güsten, R. "Carbon in different phases ([CII], [CI], and CO) in infrared dark clouds: Cloud formation signatures and carbon gas fractions" A&A 571A, 53B (Nov. 2014)
- [38] Miyata, Takashi et al. "The University of Tokyo Atacama Observatory 6.5m telescope: project status 2022" in [Millimeter, Submillimeter, and Far-Infrared Detectors and Instrumentation for Astronomy XI], Society of Photo-Optical Instrumentation Engineers (SPIE) Conference Series 12190-4 (July 2022).
- [39] Higgins, Ronan et al. "LoRaWAN usage for remote telescope operations" in [Millimeter, Submillimeter, and Far-Infrared Detectors and Instrumentation for Astronomy XI], Society of Photo-Optical Instrumentation Engineers (SPIE) Conference Series 12190-4 (July 2022).